Supporting Information

Design Criteria for the Competing Chlorine and Oxygen Evolution Reactions: Avoid the OCl Adsorbate to Enhance Chlorine Selectivity

Kai S. Exner[1,*]

[1] *Sofia University, Faculty of Chemistry and Pharmacy, Department of Physical Chemistry, 1 James Bourchier Avenue, 1164 Sofia, Bulgaria*

* Corresponding author: kai.exner@alumni.uni-ulm.de

ORCID: 0000-0003-2934-6075

1 ESSI-Descriptor Activity Maps: General Approach and Oxygen Evolution Reaction

The concept of ESSI-descriptor activity maps was introduced by the author in recent contributions.[1-3] The central idea of this unifying approach is to connect different perspectives in the field of oxygen evolution (OER) electrocatalysis (cf. main text, **Figure 1**). The commonly applied material screening approach in the literature relies on the assessment of binding energies, in that the concept of linear scaling relationships in conjunction with a conventional volcano analysis is used to comprehend trends in a homologous series of materials.[4] Despite of the success of this simple notion, critical voices argue that the simple volcano method cannot always reproduce activity trends correctly.[5,6] The author traces this to the finding that the applied overpotential and kinetics are not accounted for in the conventional volcano methodology.[7]

Rossmeisl and co-workers suggested that the OER over transition-metal oxides proceeds by four electron-proton coupled transfer steps, in which the OH, O, and OOH adsorbates are stabilized on the active metal site, M (cf. equations (1) – (4)).[8] Rutile transition-metal oxides with (110) surface orientation reveal two kinds of undercoordinated surface atoms, namely one-fold undercoordinated metal sites (M_{cus}) and one-fold undercoordinated oxygen atoms (O_{br}).[9] It has been demonstrated in the literature that the M_{cus} sites are the underlay for the oxygen and chlorine evolution reactions.[8,10-16] Adsorbates on the M_{cus} sites are marked by the subscript "ot". **Figure S1** depicts the fully-oxygen covered surface structure of a transition-metal oxide, $MO_2(110)$, and equations (1) – (4) indicate the proposed reaction mechanism for the OER.

$$H_2O_{(l)} + M_{cus} \rightarrow M_{cus}\text{-}OH_{ot} + H^+ + e^- \qquad \Delta G_1 \qquad (1)$$

$$M_{cus}\text{-}OH_{ot} \rightarrow M_{cus}\text{-}O_{ot} + H^+ + e^- \qquad \Delta G_2 \qquad (2)$$

$$M_{cus}\text{-}O_{ot} + H_2O_{(l)} \rightarrow M_{cus}\text{-}OOH_{ot} + H^+ + e^- \qquad \Delta G_3 \qquad (3)$$

$$M_{cus}\text{-}OOH_{ot} \rightarrow M_{cus} + O_{2(g)} + H^+ + e^- \qquad \Delta G_4 \qquad (4)$$

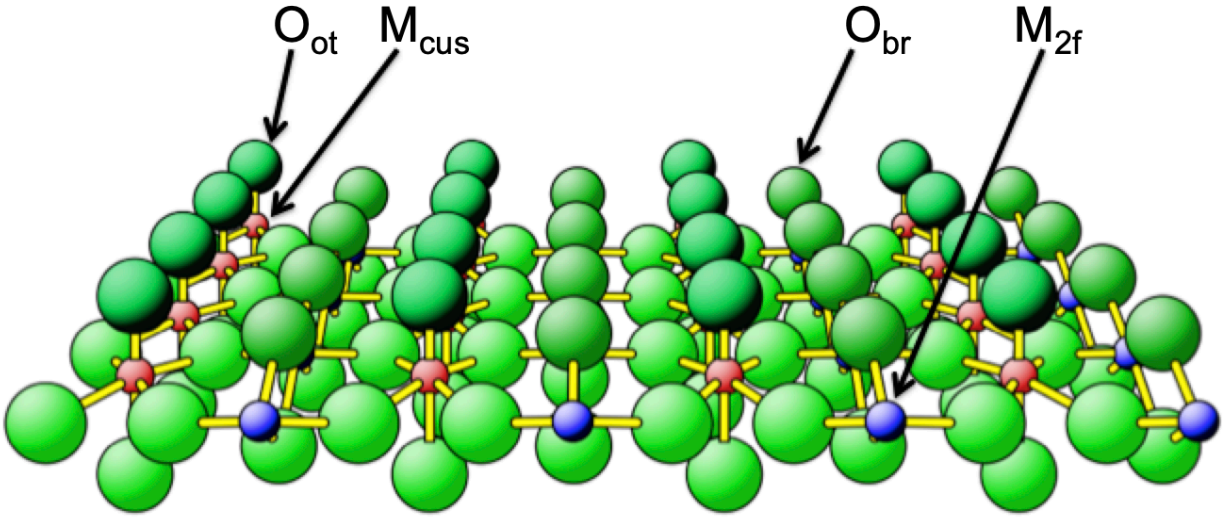

Figure S1. Fully-oxygen covered transition-metal oxide $MO_2(110)$ surface. The mechanistic processes of the oxygen (OER) and chlorine (CER) evolution reactions proceed on the one-fold undercoordinated metal atoms, M_{cus}, or on adsorbates that cap the M_{cus} sites. Under the anodic conditions of the OER and CER, the M_{cus} sites are typically capped by surface oxygen (O_{ot}), as indicated in the figure. The M_{2f} sites are connected to two oxygen atoms in a bridging position (O_{br}), and thus are not involved in elementary steps of the OER and CER.

The conventional volcano method relies on the assessment of the free-energy changes ΔG_j (j = 1, 2, 3, 4) of equations (1) – (4). Most notably, a scaling relation has been reported that intrinsically couples the free-energy changes ΔG_2 and ΔG_3, thus thermodynamically restraining the OER:[4]

$$\Delta G_3 = -\Delta G_2 + B \qquad (5)$$

For the offset, B, in equation (5), values ranging from 2.8 eV up to 3.4 eV can be found in the literature.[2,4,17,18] As such, the offset also depends on the investigated class of materials.[1]

The thermodynamic approach of the scaling relations has been extended by incorporating the applied overpotential and kinetics into the analysis, putting forth the concepts of overpotential-dependent volcano plots[19,20] and kinetic scaling relations.[21,22] The concept of kinetic scaling relations connects the assessment of the linear scaling relationships to a single experimental input parameter; that is, the threshold electrode potential, at which the experimental Tafel slope, b, exceeds 59 mV/dec. in a class of materials. Applying the microkinetic model of Over and Exner,[23] the combination of the scaling relations with the Tafel slope enables resolving the active surface termination of the electrode material and the rate-determining reaction step under typical reaction conditions. For the OER over transition-metal oxides, it was demonstrated that either the formation or the decomposition of the OOH adsorbate (cf. equations (3) – (4)) is rate determining under OER conditions ($\eta_{OER} > 0.40$ V).[21] This finding also holds true for general metal oxides.[3] Therefore, the kinetics of the OER for these classes of materials can be simplified, since the OOH adsorbate corresponds to the key intermediate in the mechanistic processes. Then,

the concept of overpotential-dependent volcano plots enables specifying the location of the volcano's apex for the OOH intermediate as central adsorbate by factoring the applied overpotential into the assessment of the scaling relation (cf. equation (5)).[1,20] The outcome of the overpotential-dependent volcano plot is linked to the concept of the electrochemical-step symmetry index (ESSI), as introduced by Calle-Vallejo and co-workers,[24,25] and given by the following formula:

$$\mathrm{ESSI} = \frac{1}{n}\sum_{k=1}^{n}\left(\frac{\Delta G_k^+}{e} - 1.23\ \mathrm{V}\right) \tag{6}$$

In equation (6), e denotes the elementary charge. Referring to the ESSI, it needs to be emphasized that the sum in equation (6) addresses only free-energy changes ΔG_k^+ that exceed the (standard) equilibrium potential of the OER, U^0_{OER} = 1.23 V, on a potential scale, that is, $\Delta G_k^+ / e > 1.23$ V, whereas free-energy changes $\Delta G_k^- / e \leq 1.23$ V are not taken into account.

The general strategy to construct ESSI-descriptor activity maps is compiled in **Figure S2**. As descriptor for the OER, commonly the free-energy change ΔG_2 (cf. equation (2)) is used since this descriptor has shown to reproduce activity trends in the OER correctly.[1,20,26] Compared to the conventional volcano methodology, the ESSI-descriptor activity map relies on the same computational costs, but includes an additional experimental input parameter into the analysis, which is needed to resolve the rate-determining step and the key intermediate by the concept of kinetic scaling relations. In this context, it has been shown that, instead of conducting a Tafel analysis for selected electrode materials, it is also feasible to use as experimental input parameter the threshold overpotential at which the current density for the most promising electrocatalysts exceeds 10 mA/cm^2. This enables high-throughput screening at low experimental and computational costs, and simplifies the analysis.[1,3]

The ESSI-ΔG_2 activity map for the OER over transition-metal oxides at an applied overpotential of $\eta_{\mathrm{OER}} = U - U^0_{\mathrm{OER}}$ = 0.40 V is depicted in **Figure S3**. Following the discussion in reference **1**, three different areas can be distinguished. The free-energy regime of 1.03 eV < ΔG_2 < 1.43 eV in conjunction with ESSI < 0.45 V (green color) is suggested as optimum situation, thereby considering the thermodynamic limitation due to the scaling relations (cf. equation (5)). The yellow highlighted area, ΔG_2 < 1.03 eV or ΔG_2 > 1.43 eV in conjunction with ESSI < 0.45 V, corresponds to potentially active OER catalysts, but, due to binding oxygen either too strongly or too weakly, this free-energy range does not refer to the apex of the overpotential-dependent volcano plot at typical OER conditions of η_{OER} > 0.40 V. Independent of ΔG_2, it has been shown that for ESSI > 0.45 V (red color) the strong deviation from catalytic symmetry might result in poor OER activity so that these electrode materials can be discarded.[1,2]

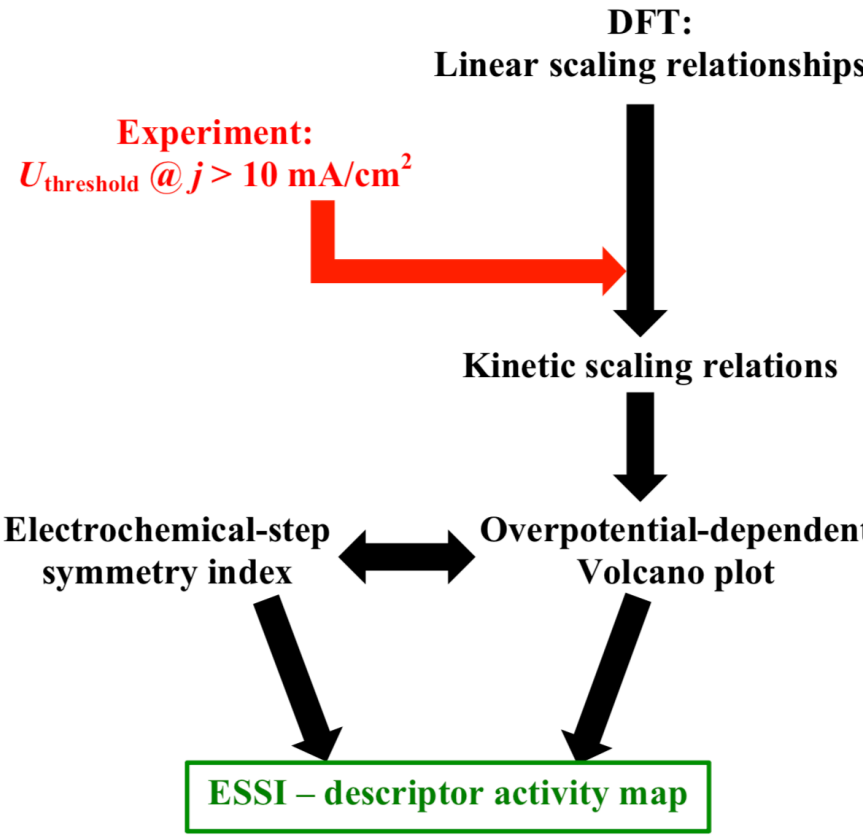

Figure S2. Methodology to construct ESSI-descriptor maps based on the combination of density functional theory (DFT) calculations and a single experimental input parameter. The unifying concept takes, besides simple binding energies, the kinetics, applied overpotential, and catalytic symmetry into consideration.[1-3]

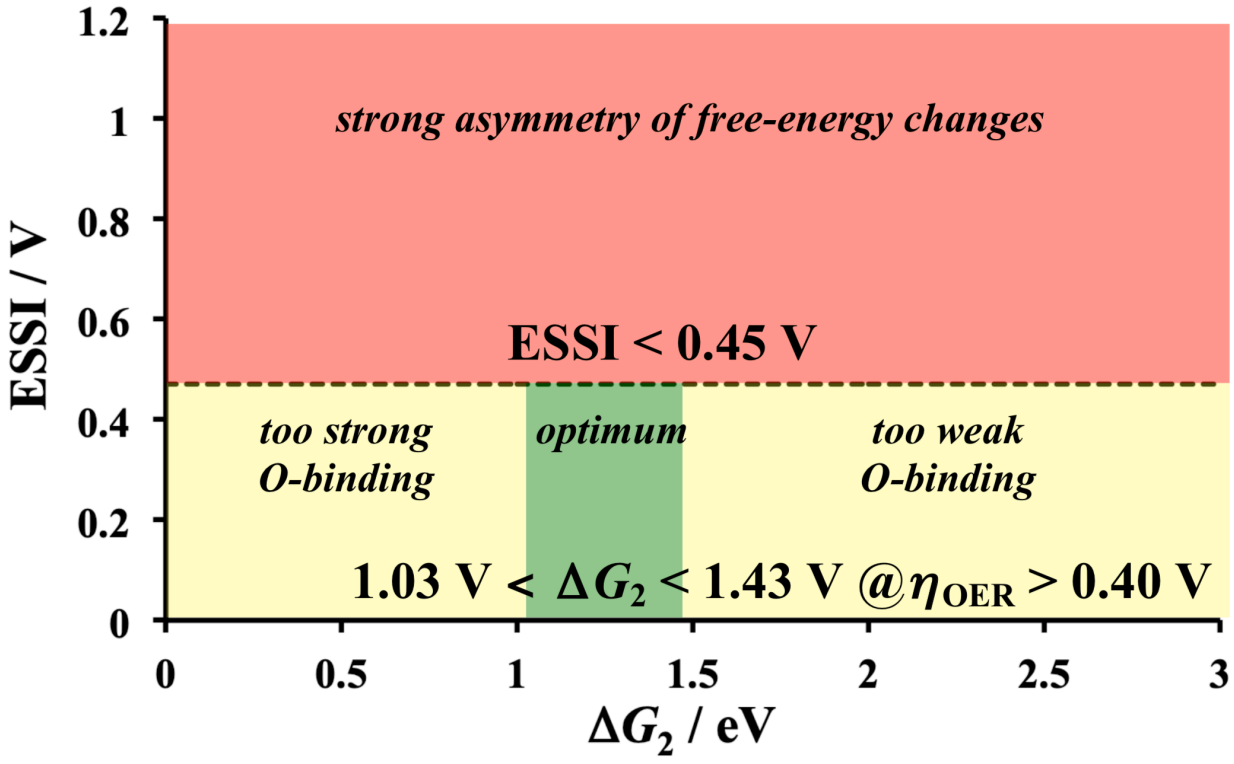

Figure S3. ESSI-ΔG_2 activity map for the OER over transition-metal oxides at η_{OER} = 0.40 V. The different colors in the figure differentiate between highly active electrode materials (green), potentially active electrocatalysts (yellow), and inactive electrode compositions (red).

The chlorine evolution reaction (CER) is an anodic process that competes with the OER in case that the aqueous, acidic electrolyte solution contains chloride anions.[13,27,28] The CER is a two-electron process with a fast kinetics: $2\ Cl^-_{(aq)} \rightarrow Cl_{2(g)} + 2\ e^-$, $U^0_{CER} = 1.36$ V *vs*. SHE (standard hydrogen electrode).[29] In contrast, the OER is thermodynamically preferred over the OER, but its kinetics is much slower due to the transfer of four electrons: $2\ H_2O_{(aq)} \rightarrow O_{2(g)} + 4\ H^+_{(aq)} + 4\ e^-$, $U^0_{OER} = 1.23$ V *vs*. RHE (reversible hydrogen electrode).[30] In order to address the selectivity problem of the competing CER and OER, an overpotential of $\eta_{CER} = U - U^0_{CER} = 0.05$ V is used in the analysis; this overpotential corresponds to $\eta_{OER} = 0.18$ V when referring to a pH value of zero (pH = 0). As such, the ESSI-ΔG_2 activity map for the OER over transition-metal oxides in **Figure S3** needs to be translated from $\eta_{OER} = 0.40$ V to $\eta_{OER} = 0.18$ V. The overpotential-dependent scaling relation for the OOH adsorbate, $\Delta G_3 = f(\eta_{OER})$, is given by equation (7), thereby using an offset of $B = 2.93$ eV in the analysis:[1,2]

$$\Delta G_3(\eta_{OER}) = -\Delta G_2 + 1.70\ \text{eV} - e\,\eta_{OER} \qquad (7)$$

Applying the criterion $\Delta G_3(\eta_{OER} = 0.18\ \text{V}) = 0$,[7,31] equation (7) purports as ideal free-binding energy $\Delta G_2 = 1.52$ eV. Considering error bars of ±0.2 eV,[1,2] the corresponding free-energy regime for optimum performance in the OER at $\eta_{OER} = 0.18$ V is given by $1.32\ \text{eV} < \Delta G_2 < 1.72$ eV, which is used for the analysis in the main text (cf. **Figure 2a**). It shall be noted, though, that the translation of the ESSI-ΔG_2 activity map for the OER from $\eta_{OER} = 0.40$ V to $\eta_{OER} = 0.18$ V relies on the assumption that the OOH adsorbate refers to the key intermediate in the reaction mechanism (cf. equation (1) – (4)). It has been shown that this precondition is fulfilled for $\eta_{OER} > 0.35$ V in the class of transition-metal oxides, but could be violated for $\eta_{OER} < 0.35$ V.[21] Therefore, the free-energy range of $1.32\ \text{eV} < \Delta G_2 < 1.72$ eV needs to be treated with some caution as the optimum binding-energy regime could change as soon as another adsorbate (OH or O) comes into play. The present article aims to derive a qualitative rather than a quantitative picture of the CER *vs*. OER selectivity problem. Even if the OH or O adsorbates correspond to the key intermediate, the free-energy regime for ideal performance in the OER is not significantly affected, as demonstrated in a recent contribution.[3] Therefore, we stay with the above assumption, indicating that the translation of the ESSI-ΔG_2 activity map for the OER from $\eta_{OER} = 0.40$ V to $\eta_{OER} = 0.18$ V is feasible by presuming that also in this overpotential regime the OOH adsorbate refers to the key intermediate in the entire class of transition-metal oxides.

2 ESSI-Descriptor Activity Maps for the Chlorine Evolution Reaction

In the following, the concept of ESSI-ΔG_2 activity maps is used to analyze the CER, and hence the CER *vs*. OER selectivity problem over transition-metal oxides for different mechanistic pathways. In the literature, the binding energy of oxygen, ΔE_O, has been commonly applied as descriptor to address selectivity trends in the competing CER and OER.[10,13,32-34] Recently, it has been shown that ΔG_2 might be a better descriptor than ΔE_O for this selectivity issue.[20] This is the reason why ΔG_2 instead of ΔE_O is used in the analysis.

The data set for the evaluation of selectivity trends in the class of transition-metal oxides is taken from the work of Viswanathan and co-workers.[16] The authors investigated seven transition-metal oxides (RuO_2, IrO_2, TiO_2, PtO_2, RhO_2, SnO_2, and VO_2) with (110) surface orientation. Further information can be found in the main text, Section 2.2 or in reference **16**.

2.1 OCl Pathway

Due to the harsh anodic reaction conditions, most transition-metal oxide surfaces are fully oxidized under CER/OER conditions; that is, the undercoordinated M_{cus} sites are capped by surface oxygen, O_{ot} (cf. **Figure S1**).[4,10,12-16] Thus, chlorine is able to adsorb on the active M_{cus}–O_{ot} sites, thereby forming an OCl adsorbate as precursor species (cf. equations (8) – (9)):

$$M_{cus}–O_{ot} + Cl^- \rightarrow M_{cus}–OCl_{ot} + e^- \quad (8)$$

$$M_{cus}–OCl_{ot} + Cl^- \rightarrow M_{cus}–O_{ot} + Cl_2 + e^- \quad (9)$$

In **Figure S4**, the free-formation energy of the OCl adsorbate with respect to the O-covered surface, $\Delta G_{OCl} = \Delta G(OCl) – \Delta G(O)$, is plotted as a function of the descriptor ΔG_2 for the seven transition-metal oxide MO_2(110) surfaces, thereby considering the influence of neighboring adsorbates on the energetics. The corresponding linear scaling relation is given by equation (10):

$$\Delta G_{OCl} = – 0.93 \cdot \Delta G_2 + 2.37 \text{ eV} \quad (10)$$

The analysis of the optimum free-binding energy for the OCl adsorbate as key intermediate is performed in a similar fashion to the scenario of the OOH adsorbate for the OER (cf. SI, Section 1). The overpotential-dependent scaling relation amounts to:

$$\Delta G_{OCl}(\eta_{CER}) = – 0.93 \cdot \Delta G_2 + 1.01 \text{ eV} – e \cdot \eta_{CER} \quad (11)$$

Applying the criterion $\Delta G_{OCl}(\eta_{CER} = 0.05 \text{ V}) = 0$,[7,31] equation (11) purports as ideal free-binding energy $\Delta G_2 = 1.03$ eV. Considering error bars of ±0.2 eV, the corresponding free-energy regime for optimum performance in the CER via the OCl adsorbate at $\eta_{CER} = 0.05$ V is given by $0.83 \text{ eV} < \Delta G_2 < 1.23 \text{ eV}$, which is used for the analysis in the main text (cf. **Figure 2b**).

The ESSI for all catalysts is calculated by equation (6), but using 1.36 V instead of 1.23 V as reference potential. It needs to be emphasized, though, that in case of a two-electron process the

ESSI is identical to the thermodynamic overpotential, η_{TD}, which is commonly used as activity descriptor in the literature.[35] All data for the CER over transition-metal oxides via the OCl adsorbate is compiled in **Table S1**.

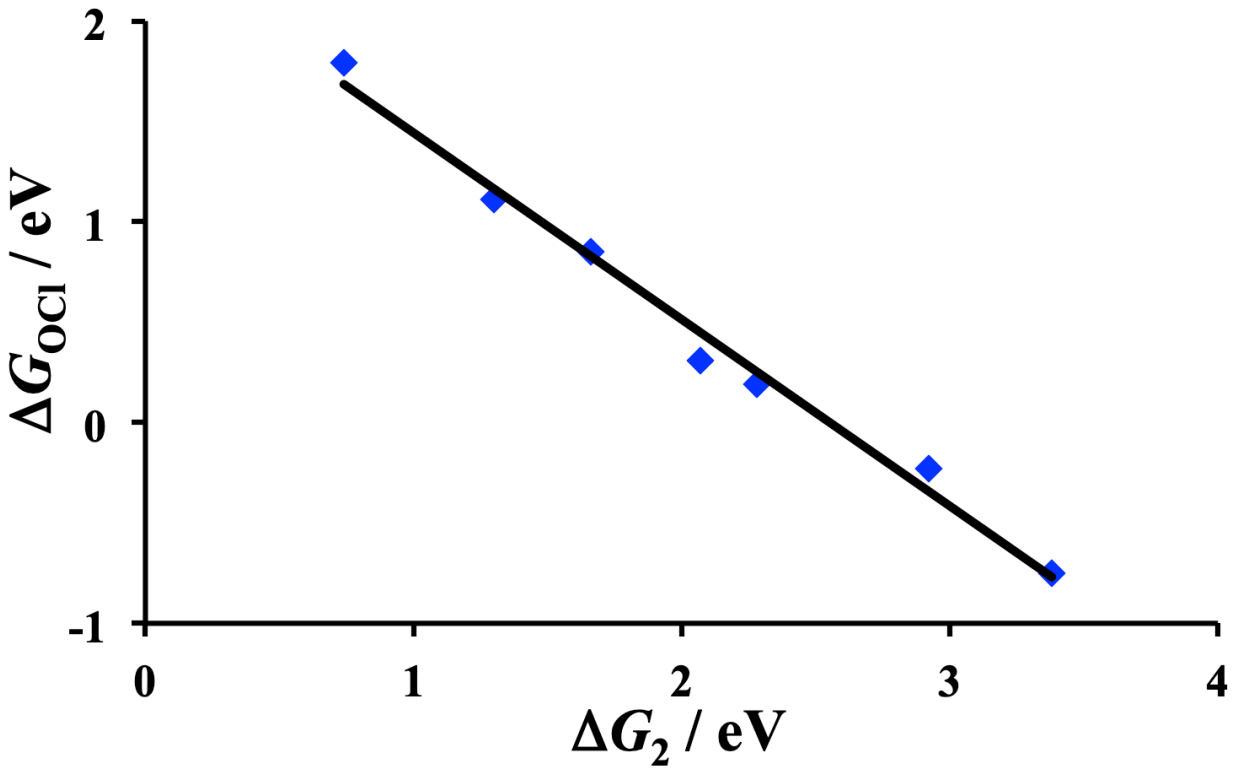

Figure S4. Linear scaling relationship between the free-binding energy of the OCl adsorbate with respect to the O-covered surface and the free-energy change ΔG_2, serving as descriptor. The best-fit function is indicated by a solid black line (cf. equation (10)).

Table S1. Free-energy change ΔG_2, free-binding energy of OCl, ΔG_{OCl}, and ESSI for MO_2(110) surfaces. The data has been adopted from DFT calculations of Viswanathan and co-workers.[16]

	ΔG_2 / eV	ΔG_{OCl} / eV	ESSI / V
RuO_2(110)	1.30	1.11	0.25
IrO_2(110)	1.66	0.85	0.51
TiO_2(110)	2.92	–0.23	1.59
PtO_2(110)	2.28	0.19	1.17
RhO_2(110)	2.07	0.31	1.05
VO_2(110)	0.74	1.79	0.43
SnO_2(110)	3.38	–0.75	2.11

2.2 ClO_2 Pathway

Rossmeisl and co-workers suggested that chlorine can also bind in-between two neighboring oxygen surface atoms that form a peroxide species $(O_2)_{ot,ot}$ between two adjacent M_{cus} atoms.[10] As a consequence, an ClO_2 adsorbate is formed as precursor species (cf. equations (12) – (13)):

$$2M_{cus}–(O_2)_{ot,ot} + Cl^- \rightarrow 2M_{cus}–(O_2)_{ot,ot}Cl + e^- \quad (12)$$

$$2M_{cus}–(O_2)_{ot,ot}Cl + Cl^- \rightarrow 2M_{cus}–(O_2)_{ot,ot} + Cl_2 + e^- \quad (13)$$

In **Figure S5**, the free-formation energy of the ClO_2 intermediate with respect to the fully O-covered surface, $\Delta G_{Cl(O2)} = \Delta G(ClO_2) – \Delta G(2O)$, is plotted as a function of the descriptor ΔG_2 for the $MO_2(110)$ surfaces. The corresponding linear scaling relation is given by equation (14):

$$\Delta G_{Cl(O2)} = – 2.82 \cdot \Delta G_2 + 5.62 \text{ eV} \quad (14)$$

The overpotential-dependent scaling relation amounts to:

$$\Delta G_{Cl(O2)}(\eta_{CER}) = – 2.82 \cdot \Delta G_2 + 4.26 \text{ eV} – e\,\eta_{CER} \quad (15)$$

Applying the criterion $\Delta G_{Cl(O2)}(\eta_{CER} = 0.05 \text{ V}) = 0$,[7,31] equation (15) purports as ideal free-binding energy $\Delta G_2 = 1.49$ eV. Considering error bars of ±0.2 eV, the corresponding free-energy regime for optimum performance in the CER via the ClO_2 intermediate at $\eta_{CER} = 0.05$ V is given by 1.29 eV < ΔG_2 < 1.69 eV, which is used for the analysis in the main text (cf. **Figure 3a**). All data addressing the ClO_2 adsorbate is compiled in **Table S2**.

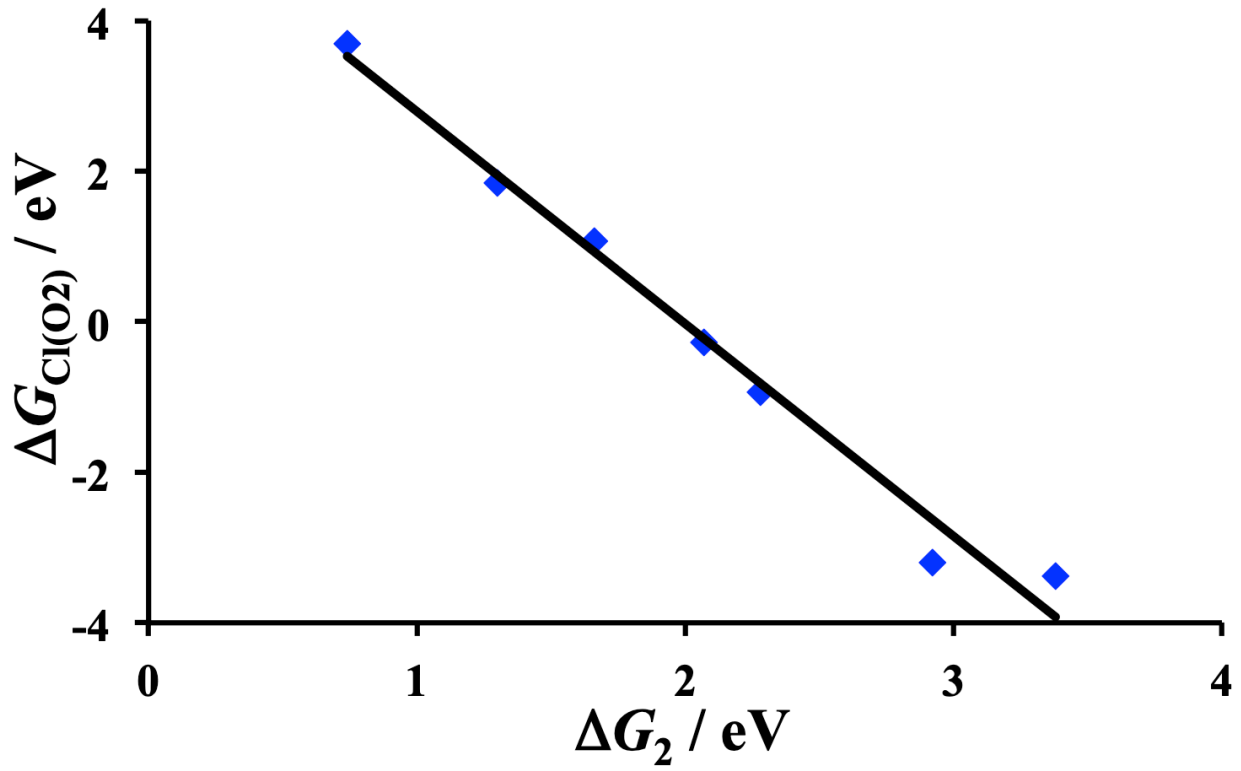

Figure S5. Linear scaling relationship between the free-binding energy of the ClO_2 adsorbate with respect to the fully O-covered surface and the free-energy change ΔG_2, serving as descriptor. The best-fit function is indicated by a solid black line (cf. equation (14)).

Table S2. Free-energy change ΔG_2, free-binding energy of ClO_2, $\Delta G_{Cl(O2)}$, and ESSI for $MO_2(110)$ surfaces. The data has been adopted from DFT calculations of Viswanathan and co-workers.[16]

	ΔG_2 / eV	$\Delta G_{Cl(O2)}$ / eV	ESSI / V
$RuO_2(110)$	1.30	1.84	0.48
$IrO_2(110)$	1.66	1.07	0.29
$TiO_2(110)$	2.92	–3.20	4.56
$PtO_2(110)$	2.28	–0.94	2.30
$RhO_2(110)$	2.07	–0.27	1.63
$VO_2(110)$	0.74	3.69	2.33
$SnO_2(110)$	3.38	–3.38	4.74

2.3 Cl Pathway

In case that the undercoordinated M_{cus} sites are not capped by surface oxygen, chlorine may directly adsorb on the underlying metal atom, resulting in the formation of a Cl adsorbate as precursor species (cf. equations (16) – (17)):

$$M_{cus} + Cl^- \rightarrow M_{cus}–Cl_{ot} + e^- \quad (16)$$

$$M_{cus}–Cl_{ot} + Cl^- \rightarrow M_{cus} + Cl_2 + e^- \quad (17)$$

In **Figure S6**, the free-formation energy of the Cl intermediate with respect to the unoccupied cus site, $\Delta G_{Cl} = \Delta G(Cl) – \Delta G(*)$, is plotted as a function of the descriptor ΔG_2 for the $MO_2(110)$ surfaces. The corresponding linear scaling relation is given by equation (18):

$$\Delta G_{Cl} = 0.53 \cdot \Delta G_2 – 0.53 \text{ eV} \quad (18)$$

The overpotential-dependent scaling relation amounts to:

$$\Delta G_{Cl}(\eta_{CER}) = 0.53 \cdot \Delta G_2 – 1.89 \text{ eV} – e\,\eta_{CER} \quad (19)$$

Applying the criterion $\Delta G_{Cl}(\eta_{CER} = 0.05 \text{ V}) = 0$,[7,31] equation (19) purports as ideal free-binding energy $\Delta G_2 = 3.66$ eV. Considering error bars of ±0.2 eV, the corresponding free-energy regime for optimum performance in the CER via the Cl intermediate at $\eta_{CER} = 0.05$ V is given by $3.46 \text{ eV} < \Delta G_2 < 3.86$ eV, which is used for the analysis in the main text (cf. **Figure 3b**). All data addressing the Cl adsorbate is compiled in **Table S3**.

It shall be noted that there is some scattering of the data points around the fit function in **Figure S6**. However, even if the offset of the fit function in equation (18) is varied by 0.50 eV, it does not have a qualitative impact on the main result, namely that the optimum free-binding energy regime for the Cl intermediate is located at weak oxygen bonding (large values of ΔG_2). Assuming that the intercept of the scaling relation in equation (18) amounts to –1.03 eV or –0.03

eV (instead of –0.53 eV) the ideal free energy of ΔG_2 is given by 4.60 eV or 2.72 eV, respectively. Both values are still far above the optimum OER range (1.32 eV < ΔG_2 < 1.72 eV; cf. main text, **Figure 2a**), corroborating the finding that the pathway via the Cl intermediate offers a promising path to enhanced CER selectivity. This aspect is discussed in further detail within Section 3 of the SI.

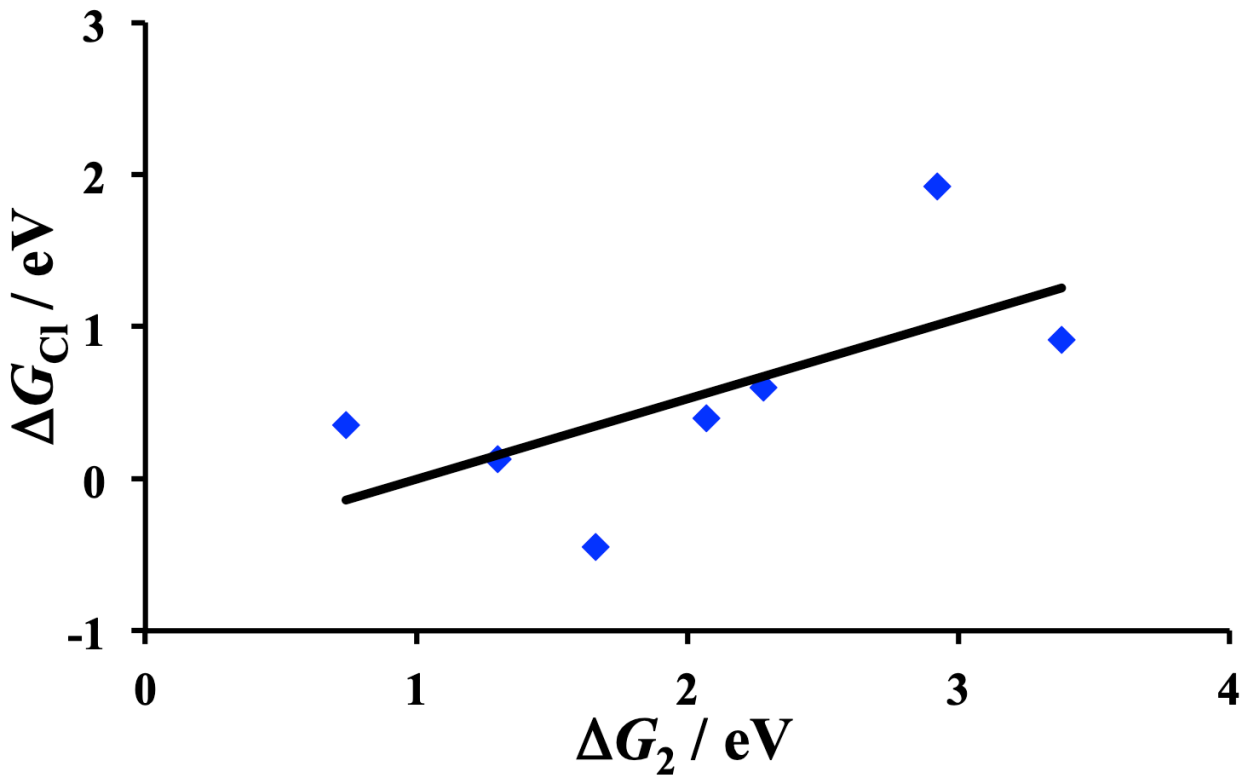

Figure S6. Linear scaling relationship between the free-binding energy of the Cl adsorbate with respect to the unoccupied cus site and the free-energy change ΔG_2, serving as descriptor. The best-fit function is indicated by a solid black line (cf. equation (18)).

Table S3. Free-energy change ΔG_2, free-binding energy of Cl, ΔG_{Cl}, and ESSI for MO_2(110) surfaces. The data has been adopted from DFT calculations of Viswanathan and co-workers.[16]

	ΔG_2 / eV	ΔG_{Cl} / eV	ESSI / V
RuO_2(110)	1.30	0.13	1.23
IrO_2(110)	1.66	–0.45	1.81
TiO_2(110)	2.92	1.92	0.56
PtO_2(110)	2.28	0.60	0.76
RhO_2(110)	2.07	0.40	0.96
VO_2(110)	0.74	0.35	1.01
SnO_2(110)	3.38	0.91	0.45

2.4 Discussion of the CER Pathways

The analysis of the ESSI-ΔG_2 activity maps (cf. main text, **Figure 2** and **Figure 3**) reveals that VO_2, RuO_2, and IrO_2 favor the OCl adsorbate in the CER, whereas all other transition-metal oxides show a tendency to form the Cl intermediate (cf. main text, Section 3.2). Viswanathan and co-workers studied the uncertainty of the mechanistic CER pathways for transition-metal oxides, using ΔE_O as descriptor.[16] When comparing the results of the authors (Figure 4 in reference **16**) to the approach of ESSI-ΔG_2 activity maps, it turns out that the outcome coincide qualitatively, independent of using ΔE_O or ΔG_2 as descriptor in the analysis. The only minor difference in the study of Viswanathan and co-workers refers to the fact that for RhO_2 the pathway via the ClO_2 adsorbate could appear feasible, whereas the present study indicates that RhO_2 favors the Cl intermediate.

It shall be noted that a similar finding was reported by the author recently, demonstrating that ΔE_O and ΔG_2 provide qualitatively the same results when discussing activity trends in the CER.[20] This emphasizes that the usage of ΔG_2 as activity descriptor for the CER *vs*. OER selectivity problem mainly refers to describe activity trends in the OER correctly, since the usage of ΔE_O can lead to erroneous results.[20,26]

3 Quantifying Chlorine Selectivity

The selectivity of the competing CER and OER is quantified by applying the model reported in reference **34**. The CER and OER are described by a Butler-Volmer type kinetics.[15,36,37] Assuming that the density of active sites for different $MO_2(110)$ surfaces is identical (i.e., focusing on the intrinsic activity), the ratio of the CER and OER current densities, j_{CER}/j_{OER}, at $\eta_{CER} = 0.05$ V and pH = 0 is given by equation (20):

$$\frac{j_{CER}(\eta_{CER} = 0.05\ \text{V})}{j_{OER}(\eta_{OER} = 0.18\ \text{V})} = \text{Exp}\left(\frac{G^{\#}_{OOH} - G^{\#}_{CER}}{k_B \cdot T}\right) \quad (20)$$

In equation (20), k_B denotes Boltzmann's constant, and T the absolute temperature in Kelvin ($T = 298.15$ K). Following the discussion in Section 1 of the SI, for the construction of the ESSI-ΔG_2 activity map it is assumed that the OOH adsorbate corresponds to the key intermediate. Thus, the transition-state free energy of the OOH intermediate, $G^{\#}_{OOH}$, may govern the OER kinetics, while for the CER the transition-state free energy, $G^{\#}_{CER}$, may refer either to the OCl adsorbate or the Cl intermediate, whereas the ClO_2 precursor was already excluded (cf. discussion in the main text, Section 3.2).

The free-energy distance of the transition-state free energies, $G^{\#}_{OOH} - G^{\#}_{CER}$, is approximated by assuming a linear decrease of the free-energy spacing of the OOH adsorbate and the CER precursor along the reaction coordinate. Assuming that the activated complexes of the CER and

OER are located in the middle of the electrochemical double layer ($\alpha_{CER} = \alpha_{OER} = ½$), the following relation holds true (cf. equation (21)):[34]

$$G^{\#}_{OOH} - G^{\#}_{CER} = \frac{1}{2} \cdot (\Delta G_{OOH} - \Delta G_{CER}) \quad (21)$$

The free-energy difference $\Delta G_{OOH} - \Delta G_{CER}$ is determined from the ESSI-ΔG_2 activity maps of the OER and CER, respectively. While for the OCl adsorbate the optimum free-binding energy amounts to $\Delta G_2 = 1.03$ eV, the OOH adsorbate is located at $\Delta G_2 = 1.52$ eV. Considering error bars of ±0.2 eV, we obtain $\Delta G_{OOH} - \Delta G_{OCl} = 1.52$ eV – 1.03 eV – 0.2 eV = 0.29 eV, and thus $G^{\#}_{OOH} - G^{\#}_{OCl} = 0.145$ eV.

The CER selectivity is determined by applying equation (22):[34]

$$\text{CER Selectivity} = \frac{\text{Exp}\left(\frac{G^{\#}_{OOH} - G^{\#}_{CER}}{k_B \cdot T}\right)}{\text{Exp}\left(\frac{G^{\#}_{OOH} - G^{\#}_{CER}}{k_B \cdot T}\right) + 1} \quad (22)$$

For the OCl adsorbate at $\eta_{CER} = 0.05$ V and pH = 0, it follows: CER selectivity = 99.6%.

In the following, the pH dependency is discussed. The free energy of the OOH adsorbate is reduced by about 0.06 eV relative to the OCl intermediate as soon as the proton activity is decreased by a factor of 10 (due to the fact that the OER equilibrium potential is pH dependent, whereas the CER equilibrium potential is not a function of the pH). As such, the difference $G^{\#}_{OOH} - G^{\#}_{OCl}$ is reduced by 0.03 eV per pH unit for pH > 0. **Table S4** summarizes the CER selectivity of the OCl adsorbate at $\eta_{CER} = 0.05$ V in dependence of the pH. It becomes evident that the CER selectivity significantly deteriorates with increasing pH (cf. **Figure 4b** of the main text).

Table S4. CER selectivity for the pathway via the OCl intermediate as a function of the pH value.

	pH = 0	**pH = 1**	**pH = 2**	**pH = 3**	**pH = 4**	**pH = 5**	**pH = 6**	**pH = 7**
CER selectivity/%	99.6	98.9	96.5	89.5	72.6	45.2	20.4	7.4

In reference **34**, the CER selectivity of RuO_2(110) was investigated. For RuO_2(110), the free-energy difference $\Delta G_{OOH} - \Delta G_{OCl}$ amounts to 0.20 eV, and thus $G^{\#}_{OOH} - G^{\#}_{OCl} = 0.10$ eV.[34] The CER selectivity of the RuO_2(110) model electrode as a function of the pH is compiled in **Table S5**, indicating that there is some room to optimize the selectivity toward the CER compared to the optimum scenario of the OCl adsorbate, discussed above (cf. **Figure 4b** of the main text). Several studies in the literature addressed this task and reported different strategies to enhance the CER selectivity of RuO_2-based electrodes.[13,34,38,39] However, the selectivity could be

even more improved to the side of the CER as soon as the mechanistic processes involve the Cl adsorbate rather than the OCl adsorbate.

Table S5. CER selectivity for RuO_2(110) as a function of the pH value. Data adopted from reference **34**.

	pH = 0	**pH = 1**	**pH = 2**	**pH = 3**	**pH = 4**	**pH = 5**	**pH = 6**	**pH = 7**
CER selectivity/%	98.0	93.8	82.6	59.6	31.5	12.5	4.3	1.4

In order to address the CER selectivity for the pathway via the Cl intermediate, the above model needs to be refined. This is due to the fact that for the OCl and OOH adsorbates as key intermediates the O-covered surface is their common reference phase, whereas the Cl adsorbate requires the unoccupied cus site as active surface site. The following strategy is applied: the average free-energy change ΔG_1 (cf. equation (1)) for the seven transition-metal oxides in the work of Viswanathan and co-workers[16] is calculated, and amounts to 0.23 eV. The scaling relations purport $\Delta G_2 + \Delta G_3 = 2.93$ eV (cf. equation (5))) in the class of transition-metal oxides.[1] Therefore, the average free-energy change ΔG_4 (cf. equation (4)) amounts to 1.43 eV. The elementary process in equation (4) forms an unoccupied cus site, on which the CER via the Cl intermediate may occur.

The optimum free-binding energy amounts to $\Delta G_2 = 3.66$ eV for the Cl intermediate, and $\Delta G_2 = 1.52$ eV for the OOH adsorbate. Besides, the free-energy change ΔG_4 is factored in the analysis as this step is indispensably required to move from the OOH intermediate to the unoccupied cus site. Considering error bars of ±0.2 eV, it follows $\Delta G_{OOH} - \Delta G_{Cl} = 3.66$ eV – 1.52 eV – 1.43 eV – 0.2 eV = 0.51 eV, and thus $G^{\#}_{OOH} - G^{\#}_{Cl} = 0.255$ eV. The pH dependency is incorporated into the model in the same fashion as discussed for the OCl adsorbate. **Table S6** summarizes the pH-dependent CER selectivity of the Cl adsorbate at $\eta_{CER} = 0.05$ V (cf. **Figure 4b** of the main text).

Table S6. CER selectivity for the pathway via the Cl intermediate as a function of the pH value.

	pH = 0	**pH = 1**	**pH = 2**	**pH = 3**	**pH = 4**	**pH = 5**	**pH = 6**	**pH = 7**
CER selectivity/%	100.0	100.0	99.9	99.8	99.5	98.3	94.9	85.2

Finally, I would like to emphasize that the present model is a simplification of the actual CER selectivity, and thus should not be interpreted as a quantitative measure. It should also be noted that other detrimental side reactions, such as the formation of hypochlorous acid or hypochlorite,

are not accounted for in this model; these competing process may further limit CER selectivity at pH values close to a neutral solution.[40] Therefore, I would like to point out the qualitative conclusion of this study, the CER via the Cl intermediate may allow achieving higher CER selectivity compared to the pathway via the OCl adsorbate, rather than its quantitative reliability.

References

(1) Exner, K.S. Design Criteria for Oxygen Evolution Electrocatalysts from First Principles: Introduction of a Unifying Material-Screening Approach. *ACS Appl. Energy Mater.* **2019**, *2*, 7991-8001.

(2) Exner, K.S. Comparison of the Conventional Volcano Analysis with a Unifying Approach: Material Screening Based on a Combination of Experiment and Theory. *J. Phys. Chem. C* **2020**, *124*, 822-828.

(3) Exner, K.S. Universality in Oxygen Evolution Electrocatalysis: High-Throughput Screening and a Priori Determination of the Rate-Determining Reaction Step. *ChemCatChem* **2020**, *12*, 2000-2003.

(4) Man, I.C.; Su, H.-Y.; Calle-Vallejo, F.; Hansen, H.A.; Martinez, J.I.; Inoglu, N.G.; Kitchin, J.; Jaramillo, T.F.; Nørskov, J.K.; Rossmeisl, J. Universality in Oxygen Evolution Electrocatalysis on Oxide Surfaces. *ChemCatChem* **2011**, *3*, 1159-1165.

(5) Schmickler, W.; Trasatti, S. Comment on "Trends in the Exchange Current for Hydrogen Evolution" [J. Electrochem. Soc., 152, J23 (2005)]. *J. Electrochem. Soc.* **2006**, *153*, L31-L32.

(6) Quaino, P.; Juarez, F.; Santos, E.; Schmickler, W. Volcano plots in hydrogen electrocatalysis − uses and abuses. *Beilstein J. Nanotechnol.* **2014**, *5*, 846-854.

(7) Exner, K.S. Is Thermodynamics a Good Descriptor for the Activity? Re-Investigation of Sabatier's Principle by the Free Energy Diagram in Electrocatalysis. *ACS Catal.* **2019**, *9*, 5320-5329.

(8) Rossmeisl, J.; Qu, Z.-W.; Zhu, H.; Kroes, G.-J.; Nørskov, J.K. Electrolysis of Water on Oxide Surfaces. *J. Electroanal. Chem.* **2007**, *607*, 83-89.

(9) Over, H. Surface Chemistry of Ruthenium Dioxide in Heterogeneous Catalysis and Electrocatalysis: From Fundamental to Applied Research. *Chem. Rev.* **2012**, *112*, 3356-3426.

(10) Hansen, H.A.; Man, I. C.; Studt, F.; Abild-Pedersen, F.; Bligaard, T.; Rossmeisl, J. Electrochemical chlorine evolution at rutile oxide (110) surfaces. *Phys. Chem. Chem. Phys.* **2010**, *12*, 283-290.

(11) Fang, Y. H.; Liu, Z. P. Mechanism and Tafel Lines of Electro-Oxidation of Water to Oxygen on RuO_2(110). *J. Am. Chem. Soc.* **2010**, *132*, 18214-18222.

(12) Exner, K.S.; Anton, J.; Jacob, T.; Over, H. Chlorine Evolution Reaction on RuO_2(110): Ab initio Atomistic Thermodynamics Study - Pourbaix Diagrams. *Electrochim. Acta* **2014**, *120*, 460-466.

(13) Exner, K.S.; Anton, J.; Jacob, T.; Over, H. Controlling Selectivity in the Chlorine Evolution Reaction over RuO_2-Based Catalysts. *Angew. Chem. Int. Ed.* **2014**, *53*, 11032-11035.

(14) Exner, K.S.; Anton, J.; Jacob, T.; Over, H. Ligand Effects and Their Impact on Electrocatalytic Processes Exemplified with the Oxygen Evolution Reaction (OER) on RuO_2(110). *ChemElectroChem* **2015**, *2*, 707-713.

(15) Exner, K.S.; Sohrabnejad-Eskan, I.; Over, H. A Universal Approach To Determine the Free Energy Diagram of an Electrocatalytic Reaction. *ACS Catal.* **2018**, *8*, 1864-1879.

(16) Sumaria, V.; Krishnamurthy, D.; Viswanathan, V. Quantifying Confidence in DFT Predicted Surface Pourbaix Diagrams and Associated Reaction Pathways for Chlorine Evolution. *ACS Catal.* **2018**, *8*, 9034-9042.
(17) Viswanathan, V.; Hansen, H. A. Unifying solution and surface electrochemistry: limitations and opportunities in surface electrocatalysis. *Top. Catal.* **2014**, *57*, 215-221.
(18) Tao, H. B.; Zhang, J.; Chen, J.; Zhang, L.; Xu, Y.; Chen, J. G.; Liu, B. Revealing Energetics of Surface Oxygen Redox from Kinetic Fingerprint in Oxygen Electrocatalysis. *J. Am. Chem. Soc.* **2019**, *141*, 13803.
(19) Exner, K.S. Beyond the Traditional Volcano Concept: Overpotential-Dependent Volcano Plots Exemplified by the Chlorine Evolution Reaction over Transition Metal Oxides. *J. Phys. Chem. C* **2019**, *123*, 16921-16928.
(20) Exner, K.S. Overpotential-Dependent Volcano Plots to Assess Activity Trends in the Competing Chlorine and Oxygen Evolution Reactions. *ChemElectroChem* **2020**, *7*, 1448-1455.
(21) Exner, K. S.; Over, H. Beyond the Rate-Determining Step in the Oxygen Evolution Reaction over a Single-Crystalline IrO_2(110) Model Electrode: Kinetic Scaling Relations. *ACS Catal.* **2019**, *9*, 6755-6765.
(22) Exner, K.S. Beyond thermodynamic-based material-screening concepts: Kinetic scaling relations exemplified by the chlorine evolution reaction over transition-metal oxides. *Electrochim. Acta* **2020**, *334*, 135555.
(23) Exner, K.S.; Over, H. Kinetics of Electrocatalytic Reactions from First-Principles: A Critical Comparison with the Ab Initio Thermodynamics Approach. *Acc. Chem. Res.* **2017**, *50*, 1240-1247.
(24) Govindarajan, N.; Garcia-Lastra, J.M.; Meijer, E.A.; Calle-Vallejo, F. Does the breaking of adsorption-energy scaling relations guarantee enhanced electrocatalysis? *Current Opinion in Electrochemistry* **2018**, *8*, 110-117.
(25) Govindarajan, N.; Koper, M.T.M.; Meijer, E.J.; Calle-Vallejo, F. Outlining the Scaling-Based and Scaling-Free Optimization of Electrocatalysts. *ACS Catal.* **2019**, *9*, 4218-4225.
(26) Seh, Z.W.; Kibsgard, J.; Dickens, C.F.; Chorkendorff, I.; Nørskov, J.K.; Jaramillo, T.F. Combining theory and experiment in electrocatalysis: Insights into materials design. *Science* **2017**, *355*, eaad4998.
(27) Kuznetsova, E.; Petrykin, V.; Sunde, S.; Krtil, P. Selectivity of Nanocrystalline IrO2-Based Catalysts in Parallel Chlorine and Oxygen Evolution. *Electrocatal.* **2015**, *6*, 198-210.
(28) Vos, J.G.; Wezendonk, T.A.; Jeremiasse, A.W.; Koper, M.T.M. MnO_x/IrO_x as Selective Oxygen Evolution Electrocatalyst in Acidic Chloride Solution. *J. Am. Chem. Soc.* **2018**, *140*, 10270-10281.
(29) Trasatti, S. Progress in the Understanding of the Mechanism of Chlorine Evolution at Oxide Electrodes. *Electrochim. Acta* **1987**, *32*, 369-382.
(30) Trasatti, S. Electrocatalysis: Understanding the Success of DSA. *Electrochim. Acta* **2000**, *45*, 2377-2385.
(31) Exner, K.S. Does a Thermoneutral Electrocatalyst Correspond to the Apex of a Volcano Plot for a Simple Two-Electron Process? *Angew. Chem. Int. Ed.* **2020**, *59*, 10236-10240.
(32) Karlsson, R.K.B.; Hansen, H.A.; Bligaard, T.; Cornell, A.; Pettersson, L.G.M. Ti atoms in $Ru_{0.3}Ti_{0.7}O_2$ mixed oxides form active and selective sites for electrochemical chlorine evolution. *Electrochim. Acta* **2014**, *146*, 733-740.
(33) Karlsson, R.K.B.; Cornell, A.; Pettersson, L.G.M., The electrocatalytic properties of doped TiO_2. *Electrochim. Acta* **2015**, *180*, 514-527.

(34) Exner, K.S. Controlling Stability and Selectivity in the Competing Chlorine and Oxygen Evolution Reaction over Transition Metal Oxide Electrodes. *ChemElectroChem* **2019**, *6*, 3401-3409.
(35) Nørskov, J.K.; Rossmeisl, J.; Logadottir, A.; Lindqvist, L.; Kitchin, J.R.; Bligaard, T.; Jonsson, H.J. Origin of the Overpotential for Oxygen Reduction at a Fuel-Cell Cathode. *J. Phys. Chem. B* **2004**, *108*, 17886-17992.
(36) Parsons, R. General equations for the kinetics of electrode processes. *Trans. Faraday Soc.* **1951**, *47*, 1332-1334.
(37) Bockris, J. O'M.; Reddy, A. K. N. Modern Electrochemistry 2A; Plenum/Rosetta Edition: New York, **1973**.
(38) Abbott, D.F.; Petrykin, V.; Okube, M.; Bastl, Z.; Mukerjee, S.; Krtil, P. Selective Chlorine Evolution Catalysts Based on Mg-Doped Nanoparticulate Ruthenium Dioxide. *J. Electrochem. Soc.* **2015**, *162*, H23-H31.
(39) Petrykin, V.; Macounova, K.; Okube, M.; Mukerjee, S.; Krtil, P. Local structure of Co doped RuO_2 nanocrystalline electrocatalytic materials for chlorine and oxygen evolution. *Catal. Today* **2013**, *202*, 63-69.
(40) Zeradjanin, A.R.; Menzel, N.; Schuhmann, W.; Strasser, P. On the faradaic selectivity and the role of surface inhomogeneity during the chlorine evolution reaction on ternary Ti–Ru–Ir mixed metal oxide electrocatalysts. *Phys. Chem. Chem. Phys.* **2014**, *16*, 13741-13747.